Interferometric Coherence Analysis of the Everglades Wetlands, South Florida

Sang-Wan Kim, *Member, IEEE*, Shimon Wdowinski, Falk Amelung, Timothy H. Dixon, and Joong-Sun Won, *Senior Member, IEEE*

***Abstract*—Interferometric synthetic aperture radar (InSAR) observations of wetlands reveal spatially detailed measurements of water-level changes and quantitative images of flow dynamics. However, lateral variability of wetland vegetation results in a heterogeneous scattering medium, which can affect interferometric coherence levels and can even limit the applicability of the technique. Here, we analyze coherence variations in Southern Florida, which consist of various wetland vegetation types, including sawgrass, graminoid, cypress, mixed shrubs, and mangrove marsh. We use JERS-1, ERS-1/2, ENVISAT, and RADARSAT-1 data, to investigate the effect of acquisition parameters and temporal baseline (time span between acquisitions) on the coherence level in the various wetland vegetation environments. The main findings of our coherence analysis are as follows: 1) Woody wetlands, such as cypress and mixed shrubs swamps, have higher coherence levels than herbaceous wetlands of sawgrass and graminoid (cattail) in all SAR data types; 2) the coherence level of C-band data is strongly dependent on temporal baseline, whereas the coherence level of L-band data depends mainly on perpendicular baseline, but to some degree also on temporal baseline; 3) backscatter from JERS-1 and RADARSAT-1 is correlated with coherence in four wetland vegetation types (sawgrass, cypress, mixed shrubs, and mangrove), but ERS backscatter has no relation to coherence, except over sawgrass marsh. Finally, our study clearly indicates that high resolution, HH polarization, and small incidence angle observations are most suitable for wetland InSAR applications.**

***Index Terms*—Backscatter, coherence, everglades, synthetic aperture radar (SAR) interferometry, vegetation, wetland.**

I. Introduction

SYNTHETIC aperture radar (SAR images) have been used for mapping delineation of wetland ecosystems by exploiting strong backscatter from forest stands under flood conditions [1]–[5]. The strong enhancement of backscatter in wetlands results from double-bounce scattering of the radar signal from the water surface and tree trunks or branches [1], [6], [7]. Backscatter investigations showed that herbaceous plants and small shrubs yielded enhanced backscatter at C-band [3], [7], and defoliated cypress-tupelo swamps gave rise to brighter returns even at Ka-band (1 cm) imagery [8]. The potential of SAR application to wetland research has benefited from the use of phase information via interferometry (InSAR), which has been related to surface water-level changes [9]–[11]. These observations are very useful for monitoring and managing wetland water resources and for detecting flow patterns. L-band (wavelength of 23.53 cm) InSAR observations of wetlands are effective for detecting dynamic water-level topography with a centimeter scale [11], [12].

While L-band SAR systems [SIR-C, JERS-1, Advanced Land Observation Satellite (ALOS)] [9], [11]–[13] have proven useful for interferometric studies of wetlands, fewer studies are available for C-band (5.6 cm) and X-band (3 cm) data. Recent studies investigated ERS-1/2 and RADARSAT C-band SAR interferometry with short acquisition intervals to reduce temporal decorrelation effects [13]–[16]. Lu and Kwoun [14] showed in Southeastern Louisiana that C-band ERS-1/2 and RADARSAT-1 InSAR data acquired over moderately dense swamp forests with a medium–low canopy closure allow to measure phase change, which is correlated with water-level change. Kim *et al.* [13] also used RADARSAT-1 and ALOS data to detect water-level changes in Louisiana wetlands. Hong *et al.* [17] have presented more recently that the high-resolution X-band TerraSAR-X data is surprisingly suitable for wetland interferometric SAR application.

The accuracy of the interferometric water-level change measurements depends on interferometric correlation coefficient (coherence). However, wetlands are heterogeneous scattering environments as wetland vegetation varies laterally in response to water availability, water depth, available nutrients, and other hydroecological constraints. Thus, it is important to understand the decorrelation properties over different vegetation types. Previous studies investigated interferometric SAR phase coherence in land cover [18], forest [19]–[21], delta ecozones [22], vegetated area and urban features [23], glaciers [24], and oyster sea-farming structures [10]. For wetlands, most previous InSAR works have focused on the interpretation of hydrological change with observed features of the interferometric phase. The one exception is the study of Lu and Kwoun [14],

Manuscript received April 25, 2011; revised November 4, 2011 and June 8, 2012; accepted October 24, 2012. This work was supported in part by Basic Science Research Program through the National Research Foundation of Korea under Grant 2011-0027244, by the NASA Cooperative Agreement under Grant NNX08BA43A (WaterSCAPES: Science of Coupled Aquatic Processes in Ecosystems from Space), and by the Department of the Interior, U.S. Geological Survey and the Florida Water Resources Research Center, University of Florida, under Grant 04HQGR0160.

S.-W. Kim is with the Department of Geoinformation Engineering, Sejong University, Seoul 143-747, Korea.

S. Wdowinski and F. Amelung are with the Division of Marine Geology and Geophysics, University of Miami, Coral Gables, FL 33124 USA.

T. H. Dixon was with the Division of Marine Geology and Geophysics, University of Miami, Coral Gables, FL 33124 USA. He is now with the Department of Geology, University of South Florida, Tampa, FL 33620-5200 USA.

J.-S. Won is with the Department of Earth System Sciences, Yonsei University, Seoul 120-749, Korea.

Color versions of one or more of the figures in this paper are available online at http://ieeexplore.ieee.org.

Digital Object Identifier 10.1109/TGRS.2012.2231418

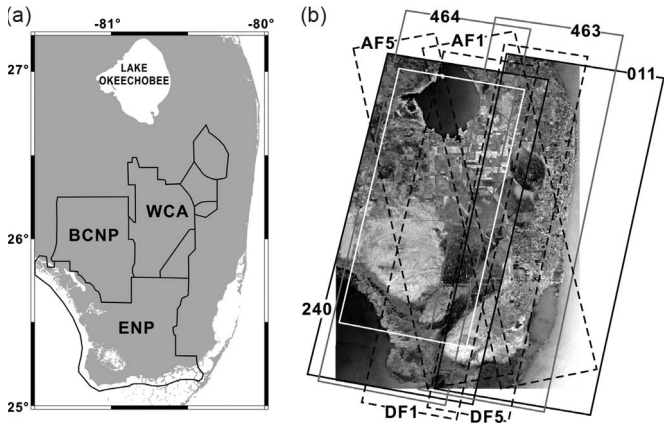

Fig. 1. (a) Location map of study area showing the general extent of the Everglades ecosystem [Everglades National Park (ENP); Big Cypress National Preserve (BCNP); Water Conservation Areas (WCA)]. (b) Ground swath map of each satellite acquisition track: thick solid lines, thin solid lines, dashed lines, and white lines represent ERS-1/2, JERS-1, RADARSAT, and ENVISAT track, respectively.

who presented quantitative coherence analysis of the southern Louisiana wetlands, but only of the C-band data.

Here, we conduct a robust coherence analysis investigating the effects of wavelength, look angle, polarization, spatial resolution, and temporal baseline (time span between acquisitions) on the coherence of various wetland vegetation types. We used JERS-1 and ERS-1/2 SAR data acquired over South Florida between 1993 and 1999, and ENVISAT ASAR and RADARSAT-1 data acquired between October 2004 and October 2005. Heretofore, we used subsets of data to study water-level changes and sheet-flow characteristics of the Everglades wetlands [11], [12], [15]. This paper focuses on the wetland InSAR technique, rather than on the hydrological application, by conducting a thorough comparative coherence analysis of the different data types. We conduct the study over South Florida because of its heterogeneous wetland environment consisting of various vegetation types. Based on the observed interferometric coherence, we evaluate empirical model describing coherence variations and establish critical parameters for the usage of wetland InSAR applications.

II. South Florida Wetlands

South Florida is one of the most suitable test sites for wetland study using remote sensing techniques because it is covered by a large wetland area characterized by a very wide, shallow, and slow sheet flow. The study area includes the Everglades National Park (ENP), Big Cypress National Preserve (BCNP), three water conservation areas (WCA), and Lake Okeechobee (see Fig. 1). The weather in South Florida consists of two seasons: wet season (May–October) and dry season (November–April). Topography is nearly flat with a maximum elevation change of 20 m.

Wetlands in the South Florida comprise mainly of freshwater marshes, freshwater swamps, and coastal mangrove estuaries (see Fig. 2). The marshes are herbaceous (treeless) wetlands dominated by vast graminoid (grasses and grass-like plants), such as cattail or sawgrass. The freshwater swamps (woody

Fig. 2. Pictures of a typical stand of four out of the five vegetation types used in this paper: Graminoid, sawgrass, cypress, and mangrove marsh.

wetlands) are composed of hardwood forest, pineland savannas, cypress forest, and prairie [25]. Most of South Florida wetlands are annually flooded for considerable periods, and some areas are continuously flooded all year round.

Sawgrass and graminoid prairie marshes are both herbaceous wetlands that differ by their vegetation type and density. Sawgrass marshes are dominated by sawgrass (> 66 %), whereas the vegetation in graminoid prairie marshes is more heterogeneous and often dominated by the invasive cattail. Sawgrass is found in a wide range of ecological settings, including estuarine and coastal grasslands [26]. In the dense sawgrass marshes, some plants reach heights of 3 m and form a near monoculture. In the sparse sawgrass marshes, the species is usually much shorter, only about a meter in height [27].

Woody wetlands consist of both freshwater swamps and saltwater mangrove forests. Cypress trees dominate the flooded freshwater environments, whereas mixed shrubs (e.g., hardwood hammock) are found in higher and drier land, such as tree islands. The mangrove vegetation composes of red and/or black mangroves, which are found along the coasts within about 10-km-wide intertidal zone. Both cypress and mangrove trees are found in South Florida wetlands as fully developed tree communities reaching height of 15–20 m, as well as dwarf communities were tree height reach only 2–3 m [26].

In this paper, we use the vegetation classification map produced by the project "Land Cover/Land Use 1999 Mapping Project," which is distributed as a vector map by the South Florida Water Management District (SFWMD) [28]. The map was produced by photointerpretation of 1999 1:40°000 scale color infrared aerial photography. We also used the National

TABLE I
LIST OF SAR DATA SETS OVER THE EVERGLADES AND ACQUISITION PARAMETERS

ERS-1/2				RADARSAT		JERS-1		ENVISAT	
Track	Date	Track	Date	Track*	Date	Track	Date	Track (Pol)+	Date
240	1993-05-03	011	1995-05-15	DF5	2004-10-06	463	1994-06-26	IS3 (HH)	2005-03-10
240	1993-06-07	011	1995-08-28	DF5	2004-10-30	463	1994-08-09	IS3 (HH)	2005-04-14
240	1995-03-22	011	1995-10-02	DF5	2004-11-23	463	1994-12-19	IS3 (HH)	2005-05-19
240	1995-05-31	011	1995-11-06	DF5	2004-12-17	463	1995-02-01	IS3 (HH)	2005-06-23
240	1995-07-05	011	1995-11-07	DF5	2005-01-10	463	1996-03-03		
240	1995-08-09	011	1995-12-11	DF5	2005-02-03	464	1993-11-19		
240	1995-09-13	011	1995-12-12	DF5	2005-02-27	464	1994-01-02		
240	1995-11-22	011	1996-01-15	DF5	2005-03-23	464	1994-05-14		
240	1995-11-23	011	1996-01-16	DF5	2005-06-27	464	1994-08-10		
240	1995-12-27	011	1996-03-26	DF5	2005-07-21	464	1994-12-20		
240	1995-12-28	011	1996-04-30	DF5	2005-10-25	464	1995-03-18		
240	1996-01-31	011	1996-06-04	DF1	2004-11-09	464	1996-01-20		
240	1996-02-01	011	1996-07-09	DF1	2005-03-09	464	1996-03-04		
240	1996-04-10	011	1996-08-13	DF1	2005-04-02				
240	1996-04-11	011	1996-09-17	AF1	2004-10-14				
240	1996-05-15	011	1996-10-22	AF1	2005-02-11				
240	1996-05-16	011	1996-11-26	AF1	2005-03-07				
240	1997-01-16	011	1997-02-04	AF1	2005-03-31				
240	1997-02-20	011	1997-03-11	AF5	2004-10-24				
240	1997-03-27	011	1997-04-15	AF5	2004-11-17				
240	1997-09-18	011	1997-05-20	AF5	2005-07-15				
240	1998-02-05	011	1997-06-24	AF5	2005-10-19				
240	1998-03-12	011	1997-07-29						
240	1998-04-16	011	1997-09-02						
240	1998-07-30	011	1997-10-07						
240	1999-05-06								

* Orbit and observation mode: DF1 and DF5 indicate descending orbit acquired with fine beam mode 1 and 5, respectively. AF1 and AF5 indicate ascending orbit acquired with fine beam mode 1 and 5, respectively.

+ Observation mode with polarization: IS3 (HH) represents narrow swath beam mode 3 with HH polarization.

Land Cover Database (NLCD) 2001 data [29], which were generated from Landsat TM imagery and distributed by the U.S. Geological Survey, as a complementary map. Although wetland plant communities change with time, we assume for simplicity that there are no great differences between the observation periods ($\sim$10 years). Seasonal change in water depth is the fastest varying biophysical parameter in the Everglades, but changes are limited. The largest changes occurring in deepest wetlands reach 1.3 m [26]. In fact, water levels in the study area have been controlled within a preset level range by the SFWMD, and consequently, the vegetation and the ecosystem have not changed much. We used the given land cover maps in order to classify the vegetation and wetland type in the various areas during our SAR observation period (1993–2005).

III. SAR DATA AND DATA PROCESSING

A. SAR Data

In this paper, we used SAR data acquired by five satellites operated by three space agencies. The L-band JERS (JERS-1) operated by the Japanese Aerospace Exploration Agency from 1992 to 1998. The C-band ERS-1 and ERS-2 and ENVISAT have been operated by the ESA (ESA) since 1992. The fifth satellite, the C-band RADARSAT-1, has been operated by the Canadian Space Agency since 1995. The data from the JERS-1 and ERS-1/2 were obtained from data archives at the Japanese and European space agencies. The ENVISAT data were acquired by ESA according to our acquisition requests. The RADARSAT data were directly received at the Center for Southeastern Tropical Advanced Remote Sensing (CSTARS), which is the University of Miami center for downlinking low-orbiting remote sensing satellite data. JERS-1 used L-band (1.28 GHz in frequency or 23.5 cm in wavelength), HH polarization, a look angle of 35°, 75-km swath width, 18-m pixel resolution, and 44 day repeat orbit. The ERS-1/2, ENVISAT, and RADARSAT-1 SAR systems operate at C-band (5.3 GHz in frequency or 5.7 cm in wavelength). ERS-1/2 have acquired VV polarization data at nominal incidence angle of 23°, 100-km ground swath width, 35 day repeat orbits, and a ground resolution of about 25 m. ENVISAT and RADARSAT-1 also acquire C-band data, but with variable acquisition parameters of different look angle pixel resolution.

Overall, we use in this paper eight swaths covering a large section of the South Florida wetlands (see Fig. 1). A

summary of all the SAR data used here is listed in Table I. Our archived data set consists of 51 concatenated ERS-1/2 SAR data (with two or three frames) acquired from two adjacent descending tracks (240 and 011) between 1993 and 1999, and 13 concatenated JERS-1 data (five-frame) from adjacent descending tracks (463 and 464) between June 1994 and March 1996. The RADARSAT-1 data set was acquired as part of a test for evaluating optimal acquisition parameters for wetland InSAR applications. We acquired 22 RADARSAT-1 fine beam mode images using four different observation modes (see Fig. 1 and Table I). The F1 and F5 modes permit high-resolution data acquisition, 6 m in range and 9 m in azimuth, with incidence angles of 37.8° and 46.7°, respectively. Four ENVISAT SAR images were also used with narrow swath 3, HH polarization, and an incidence angle of 28.7° (see Table I). RADARSAT-1 data spanned almost a full year between October 2004 and October 2005, and ENVISAT SAR data were acquired between March and June 2005.

B. Generation of Coherence and Backscatter Coefficient Images

Raw signal data were processed using the Vexcel FOCUS module [30]. The software was also used to construct an interferometric coherence map and a beta nought β_j^0 (in decibels) image. The beta nought data were converted to radar backscatter coefficient sigma nought σ^0 using the following relation [31]:

$$\sigma^0 = \beta_j^0 + 10\log_{10}(\sin I_j) \tag{1}$$

where I_j is an incidence angle as a function of Earth ellipsoid. Local topography was not taken into account for extracting sigma nought because the nearly flat terrain of the study area suggests that the effect of local incidence angle is negligible. We estimated the calibration accuracy by evaluating the mean backscatter amplitudes in urban areas. Backscatter statistics were extracted for a large sample of urban areas in the eastern part of the study area, where backscatter change between multitemporal images should be negligible if the radar calibration is properly carried out. Indeed, differences in the urban calibration site were less than 2 dB.

We calculate coherence for each interferometric pair of single-look complex (SLC) data as

$$\gamma = \frac{\left|\left\langle g_1 g_2^* e^{-i\phi}\right\rangle\right|}{\sqrt{\left\langle |g_1|^2\right\rangle \left\langle |g_2|^2\right\rangle}} \tag{2}$$

where g_1 and g_2 denote complex pixel values of two SAR images without any azimuth spectral filtering; $e^{-i\phi}$ is a phase term related to the local topography; the asterisk represents the complex conjugate; and the angular brackets represent spatial averaging over a selected window size. The range filtering to a flat surface was applied during SLC resampling before coherence estimation [32]. For each data type, different window sizes reflecting the variable acquisition resolution in azimuth and range were used to calculate coherence. We used 45 looks (15 in azimuth and 3 in range) for ERS-1/2 and ENVISAT, 27 looks (9 in azimuth and 3 in range) for JERS-1, and 36 looks (6 in azimuth and 6 in range) for RADARSAT-1, which correspond roughly to 75 m by 75 m in each satellite data. The coherence in (2) is a biased estimator depending on the actual coherence and the number of looks; therefore, the bias inherent to coherence estimator was corrected [33].

All backscatter and coherence products with radar coordinates (range–azimuth) were transformed to map coordinate [34], [35], providing an easy analysis of area statistics from multisatellite and multiimage geometry products. The coordinate error due to orbit uncertainties could be mitigated using coregistration information between real SAR and digital elevation model (DEM)-derived SAR intensity image [36]. Here, we utilized the pregeocoded SAR intensity image for image registration instead of the DEM-derived backscatter image because the topography in the study area is so even. After geocoding, an averaging of an 8×8 pixel window was performed to minimize the effects of the radiometric resolution errors. The pixel size of the final coherence and backscatter images for JERS-1, ERS-1/2 and ENVISAT was approximately 100×100 m and for RADARSAT-1 50×50 m.

IV. Coherence Analysis

A. Region Selection of Typical Wetland Vegetation Types

We selected a subset of typical land cover classes in the southern Florida wetlands in order to characterize coherence behavior according to vegetation type. Based on the 1999 Land Cover Map distributed by SFWMD and the NLCD 2001 Land Cover Map, we selected the following five principal marsh communities: cypress, mixed shrub, mangrove swamp, graminoid prairie marsh, and sawgrass marsh (see Figs. 2 and 3). All five types are perennial emergent macrophytes and are present as monospecific (containing only one species) stands or as mixtures composed of monospecific clumps. Both graminoid prairie and sawgrass marshes consist of herbaceous wetlands. Mixed shrubs are wetland hardwood communities, which are composed of a large variety of hardwood species. We also calculated the unbiased coherence values over open water to determine the level of complete decorrelation. The coherence of 0.14 to 0.16 was observed in different satellites; therefore, the value of 0.17 was set as a threshold for significant coherence values in our analysis. Cypress and mixed shrubs wetlands are located at BCNP area, mangrove swamps are located in the southern ENP along the coast, and herbaceous marshes are mostly found in WCA and ENP areas.

We selected a subset of each class with sufficiently large area from the land cover map in order to avoid the geolocation error of small stands during a geocoding process. Most parts of the wetland are subjected to seasonal effects, such as water-level change (flooded versus unflooded), soil moisture change, and phenologic change. Because we are interested in evaluating coherence variations of each wetland class with respect to various satellite parameters, it is important to use coherence-wise stable areas that are free of seasonal effects. A number of studies showed that variations in flood conditions significantly affect radar backscatter signal [3], [10], [37], [38]. The backscatter change in the southern Florida was intensively studied in the past [4], [5], [39]. For example, Kasischke *et al.* [39] reported

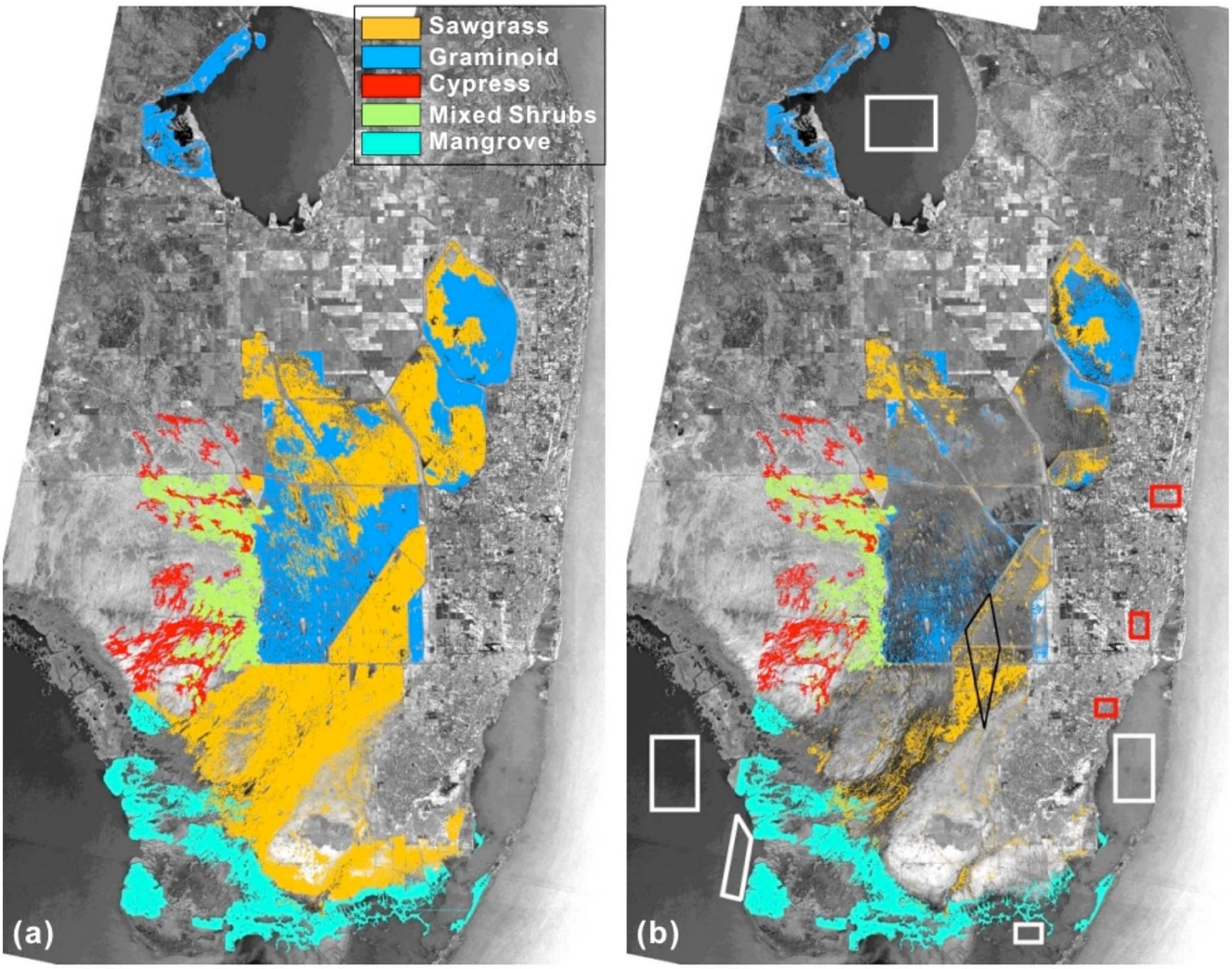

Fig. 3. Characteristic marshes in the study area superimposed on ERS multireflectivity SAR image. (a) Selected five wetland marshes based on the 1999 land cover map distributed from SFWMD and NLCD 2001 land cover map. (b) Five typical marshes with low backscattering variations (2 dB for ERS-1/2 and 2.2 dB for JERS-1 and RADARSAT) selected for statistical analysis of coherence and backscatter using ERS-1/2, JERS-1, and RADARSAT backscatter variation maps. White polygons and red polygons indicate open water surface and urban area, respectively. Backscatter and coherence are used to estimate background noisy coherence and to evaluate radar backscatter calibration accuracy. Black polygon represents sawgrass marsh covered by all of four different RADARSAT observations.

ERS-2 SAR backscatter change in the range of 1.5–5 dB, reflecting seasonal changes (mainly due to flooded/unflooded conditions). These studies also show that SAR backscatter changes are correlated with water level, soil moisture, and phenologic changes.

In order to minimize possible seasonal effects associated with the changes of seasonal water level and vegetation, we use a multitemporal backscattering response for each satellite to identify stable areas in time. Using all available imagery of each satellite, we calculated three backscatter standard deviation values in decibels, $\mathrm{SD}_{\sigma^0}^{ERS}$, $\mathrm{SD}_{\sigma^0}^{JERS-1}$, and $\mathrm{SD}_{\sigma^0}^{RADARSAT}$ for ERS-1/2, JERS-1, and RADARSAT-1, respectively. Pixels with low standard deviation values were considered as stable scatterers and were included in our analysis. We selected threshold values of 2 dB for ERS-1/2 and 2.2 dB for JERS-1 and RADARSAT to determine stable backscatter areas. A comparison between the regular and the stable scatterer vegetation cover maps (see Fig. 3) shows that most unstable scattering areas occur in sawgrass and graminoid wetlands in the southern part of WCA and ENP [difference in yellow and blue coverage between Fig. 3(a) and (b)]. Masking out these areas of high backscatter deviation minimizes potential errors of temporal decorrelation because of the decreasing effect of seasonal water-level change. We used the stable scatterers to statistically characterize the coherence and backscatter within each vegetation class. We tested the result of our stable scatterer analysis by plotting the selected area on an ERS-2 C-VV mosaic interferogram (see Fig. 4), showing that the selected areas correlate well with coherent fringe patterns.

B. Coherence Variation

1) JERS-1 Interferograms: The JERS-1 coherence variation analysis is based on 33 interferometric pairs from 13 SAR acquisitions, which are not having large spatial baseline close to critical baseline and large Doppler-centroid difference and showing mean signal more than noise level. The mean

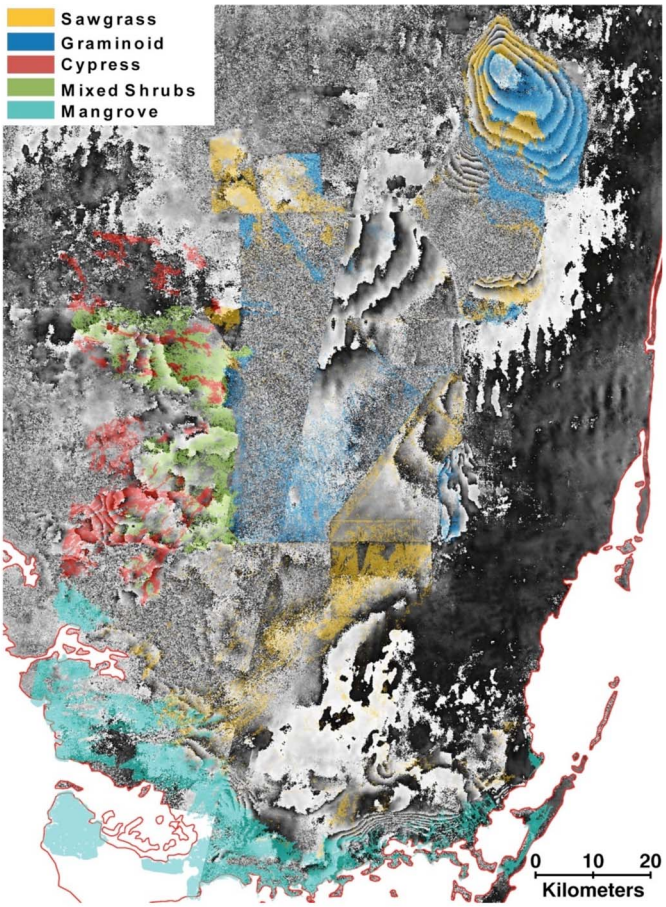

Fig. 4. Mosaic ERS-1/2 C-VV interferogram of South Florida showing phase differences occurring over a 35-day time interval and the selected areas of stable backscattering, i.e., colored according to the five marsh types. The western track (010) covers the time span of 1995/11/7_1995/12/12, and the eastern track (240) covers the 1998/2/5_1998/3/12. Fringe patterns observed in wetlands are heterogeneous and discontinuous due to man-made structures, including roads, levees and canals. The fringes represent phase shift induced by surface water-level changes.

coherence for each class was estimated by averaging the coherence values of all selected pixels.

The results of our JERS-1 coherence analysis are presented in Fig. 5 for each of the five wetland classes according to the observations' temporal (interferogram's time span) and geometrical (perpendicular) baselines. In general, the coherence is higher for cypress and mixed shrubs (0.2–0.55), intermediate for mangroves (0.2–0.5), and low for herbaceous wetlands (0.2–0.3). For JERS-1 interferometric pairs, the coherence values of all classes decrease with increasing perpendicular baseline values. Coherence values of mixed shrubs and cypress wetlands are almost independent of temporal baseline (at least up to 2.5 year), whereas those of mangrove, sawgrass, and graminoid also depend on temporal baseline. However, the temporal dependence of mangroves is different from that of herbaceous wetlands. Mangrove swamps decorrelate slowly over time, whereas herbaceous wetlands decorrelate almost abruptly after 44 days. In woody wetlands, L-band double bounce is caused by interaction between the water surface and trunks or branches, but in herbaceous wetlands, double-bounce scattering results from interaction between the water surface and the stalks or roots [1], [3], [4]. Trunks and branches do not change much over time, but stalks and roots are influenced more by changes caused by vegetation growth or scatterers movement by wind. Therefore, it is expected to find large differences between woody and herbaceous wetlands in terms of temporal decorrelation.

Coherence values can be approximated by the following model [18], [33], [40]–[43]:

$$\begin{aligned}\gamma &= \gamma_{\text{thermal}}\gamma_{\text{temporal}}\gamma_{\text{Doppler}}\gamma_{\text{volume}}\gamma_{\text{geometric}} \\ &\approx A \cdot \left(\exp^{\frac{-\Delta t}{\tau}}\right)\left(1 - \frac{\Delta f_{\text{dc}}}{B_a}\right)\left(\text{sinc}\left(\frac{k_z \Delta h}{2}\right)\right) \quad (3)\end{aligned}$$

where γ_{thermal} can be expressed by constant value A. taking into account both thermal noise and processing artifacts, and γ_{temporal}, γ_{Doppler}, γ_{volume}, and $\gamma_{\text{geometric}}$ represent a temporal, Doppler, volume, and geometric components, respectively. $\gamma_{\text{geometric}}$ can be effectively ignored because the range filtering to a flat surface was applied before coherence estimation and the slope in Everglades is close to zero [41]. Δt, $\boldsymbol{B}_a$, and Δf_{dc} are the time interval between the two data observation, the azimuth bandwidth (1555 Hz for JERS, and 900 Hz for RADARSAT-1), and the Dopper-centroid frequency difference, respectively. For γ_{volume}, a simple uniform scattering model was used, which is expressed as a function of wavenumber in the vertical direction $(k_z = (4\pi B_p)/(\lambda\rho \sin\theta))$ and canopy height variation (Δh). B_p, λ, ρ, and θ are the perpendicular baseline, wavelength, slant range, and look angle, respectively. A and τ are unknown coefficients to be estimated, which characterize the imaged surface. Although the model in (3) is not the best model, this simple one will be enough to figure out the amount of temporal decorrelation at several interested vegetation types.

We used the observed coherence values obtained for each vegetation class to constrain the model parameters using a best-fit analysis (see Table II). The analysis estimates three parameters related with thermal noise, temporal decorrelation, and volume decorrelation. The estimated temporal decorrelation parameter represents decay constant. The results of our analysis of the expected coherence values are presented in Fig. 5 by contours and grayscale areas. The expected coherence values show that, in woody wetlands (cypress and mixed shrubs), coherence is not sensitive to temporal decorrelation, whereas in herbaceous and mangrove wetlands, coherence has more dependence on temporal baselines. Mangrove has higher A of 0.42 than herbaceous wetland's values of 0.35 and 0.31. The estimated canopy height variations associated with volumetric decorrelation are very similar within 2.5–2.9 m, although the mean canopy height is different from each other. The root-mean-square errors between the measured coherence and the modeled value are less than 0.05, and the coefficients of determination R^2 are better than 0.60, except in mixed shrubs.

2) RADARSAT-1 Interferograms: The RADARSAT-1 system has an advantage of acquiring data with different incidence angles and different resolutions (modes). In this paper, we used RADARSAT-1 images acquired by four different observation modes (see Fig. 1 and Table I). In our first analysis, we do

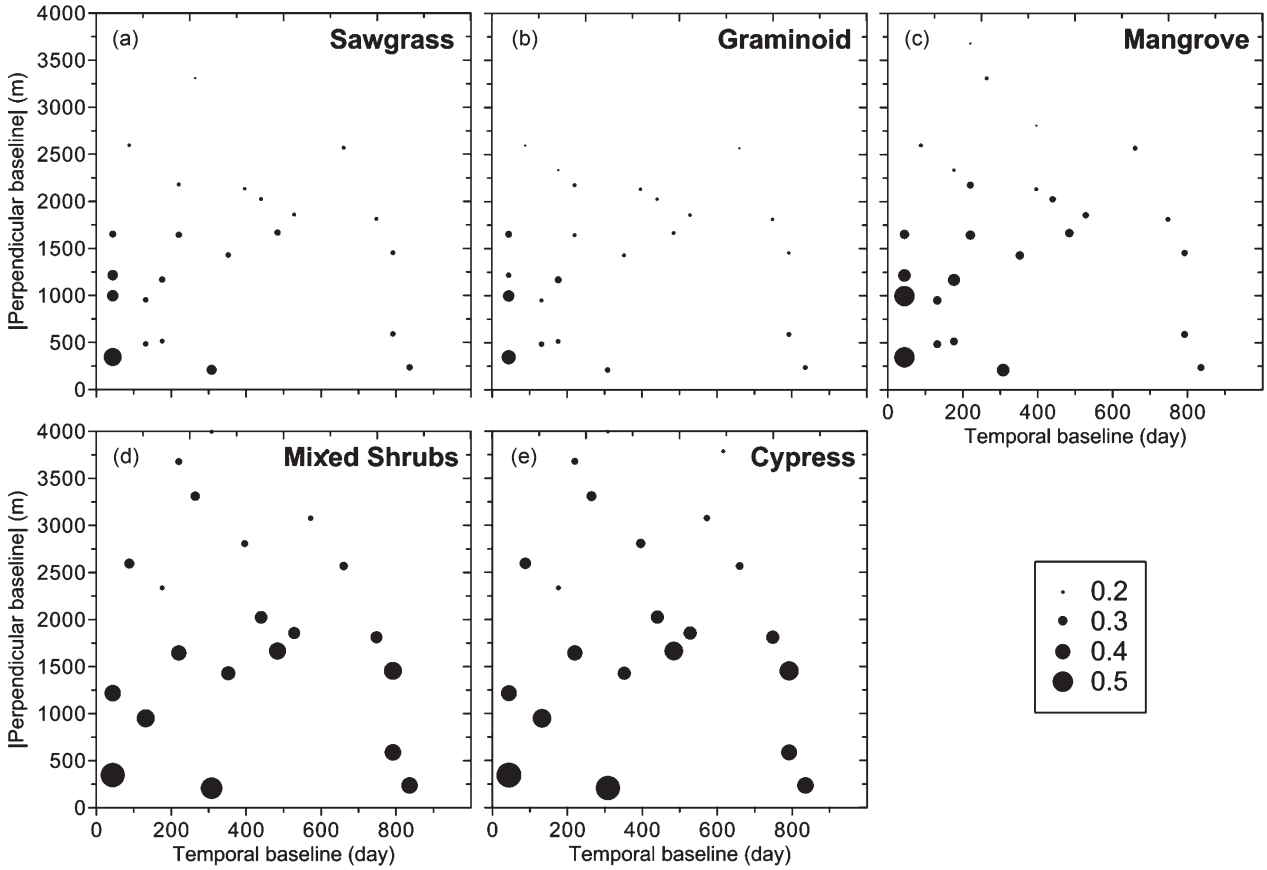

Fig. 5. JERS-1 coherence analysis results for the five wetland vegetation classes plotted as function of perpendicular and temporal baselines. Dot sizes are proportional to coherence values.

TABLE II
REGRESSION COEFFICIENT PARAMETERS RELATING COHERENCE VALUES IN (3)

Satellite	Marsh type	Estimated Parameter*			*RMSE*	R^2
		A	*τ (days)*	*Δh (m)*		
JERS-1	Sawgrass	0.35	2589.7	2.9	0.036	0.60
	Graminoid	0.31	2497.6	2.9	0.027	0.67
	Mixed Shrubs	0.43	5.1E+15	2.5	0.084	0.38
	Cypress	0.53	5887.6	2.7	0.048	0.77
	Mangrove	0.42	1830.5	2.8	0.040	0.72
RADARSAT	Sawgrass	0.26	1147.5	1.0	0.019	0.32
	Graminoid	0.28	1302.1	0.5	0.018	0.48
	Mangrove	0.33	606.8	1.3	0.031	0.45

* A, τ, and Δh are the parameters related with thermal noise, temporal decorrelation, and volume decorrelation, respectively.
RMSE: the root mean square error between coherence estimation and model value
R^2: the coefficient of determination

not distinguish between the different observation modes and present all coherence results as a function of temporal and perpendicular baselines for each wetland type (see Fig. 6). The results show that cypress, mixed shrubs, and mangrove classes have higher coherence than herbaceous wetlands. With an increasing time interval between acquisitions, coherence decreases for herbaceous wetlands and for mangrove swamps. A phenological cycle is also observable in both mixed shrubs and cypress swamps. Because the fine beam swath is narrower than the standard beam, JERS-1, and ERS-1/2 swathes, we had a limited coverage of the various class types in a single swath. The mixed shrubs and cypress sampled area were covered by only two of the four swathes, i.e., DF1 and AF5. The other three classes were covered by all four used beam modes.

Our results indicate that the coherence is strongly dependent on the temporal baseline and much less on the perpendicular one. Sawgrass marsh loses coherence rapidly with increasing time interval. In 24-day interferograms, sawgrass marsh displays a similar coherence range (0.25–0.3) to mangrove marsh,

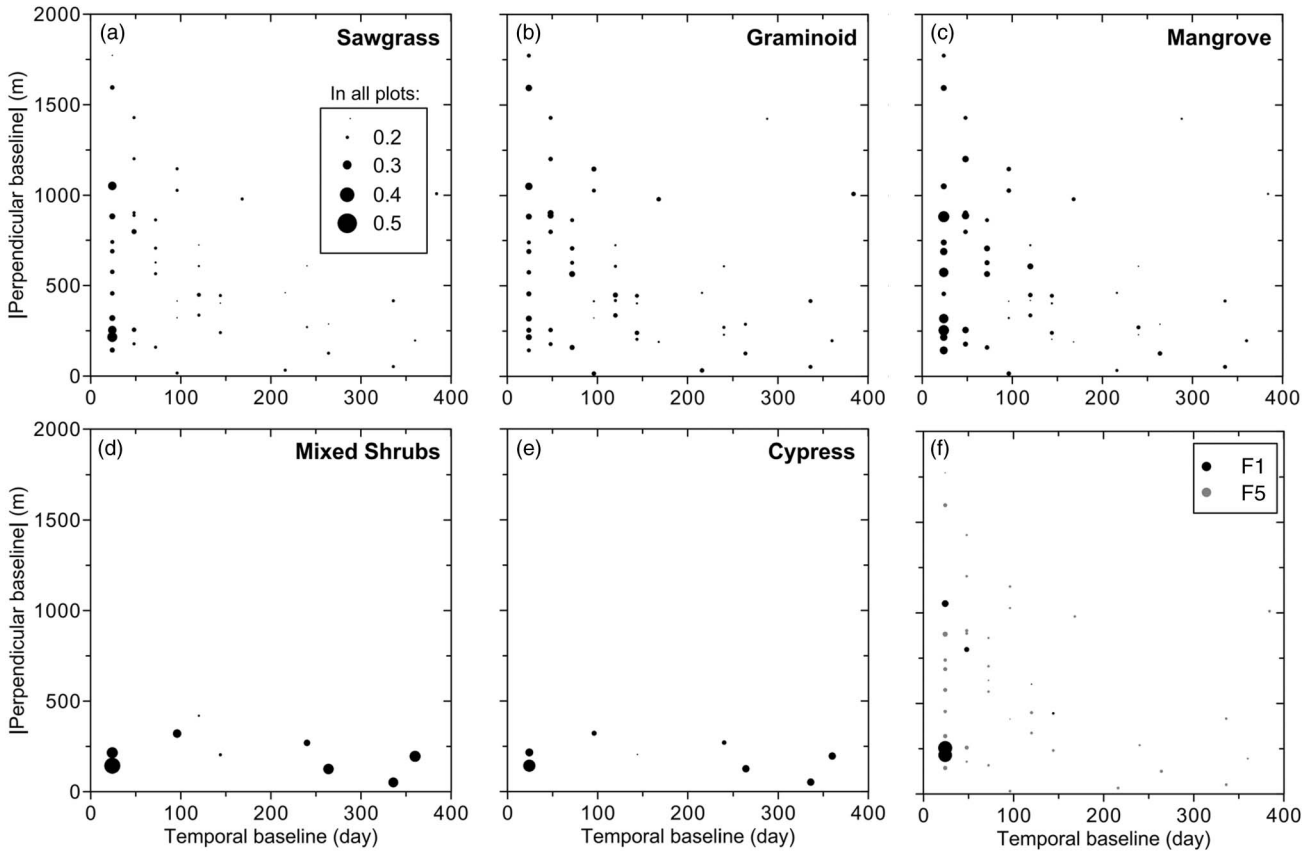

Fig. 6. (a)–(e) Scatter plot of RADARSAT coherence values for the five wetland vegetation classes. (f) Coherence for sawgrass marsh showing sensitivity of coherence values to acquisition mode. Gray and black dots represent coherence values of F1 and F5 mode data, respectively.

whereas coherence with a long time interval ($>$ 48-day) has a low value of about 0.17. The coherence of graminoid class is slightly larger (about 0.25) than that of sawgrass and is comparable with the coherence of mangrove. Similar to the JERS-1 analysis, we use our coherence model (3) to calculate expected coherence values in three of the five wetland classes: sawgrass, graminoid, and mangrove. The model was ineffective for the other two classes because of the narrow range of the perpendicular baseline in mixed shrubs and cypress. Although the R^2 for RADARSAT is not as good as JERS-1, the point is that the model results show strong dependence of the temporal baseline (see Fig. 6), which is in sharp contrast to the JERS-1 L-band results (see Fig. 5). The effect of incidence angle on the interferometric coherence is important for determining the most suitable acquisition parameters for wetland monitoring. While the variation in backscattering power with incidence angle has been widely known [7], [44], [45], the characteristics of interferometric coherence in wetlands have not been studied. Proper assessment of incidence angle effects requires nearly simultaneous acquisition at a single area. The sawgrass wetland in Fig. 3 was fortunately covered by four different acquisition modes. However, we could only use the Fine beam mode 5 (F5) descending acquisitions for this analysis because the number of ascending acquisitions is too small for statistical analysis. The descending data set can be divided into two groups: F1 with incidence angle of 37.8° and F5 with incidence angle of 46.7° [see Fig. 6(f)]. Our results show significant differences only with short temporal baselines. The three 24-day F1 interferograms have higher coherence values than the F5 interferograms. However, there is no difference between F1 and F5 coherence in interferograms with a longer period. A possible explanation for this observed difference is that the smaller incidence angles allow better vegetation penetration with less energy loss along the radiation path and consequently increasing the potential for double-bounce interactions with water surface and stem. However, our result is only preliminary because it is based on a small number of F1 mode observations, as well as only a single vegetation class. In addition, we cannot exclude the possibility of seasonal effect due to different acquisitions times. In fact, four F1 mode data used to form the two pairs with the highest coherence were acquired in the time period between March 7, and April 2, 2005. Therefore, further analysis using more SAR acquisitions is needed for better conclusive results.

3) ERS-1/2 Interferograms: Our ERS-1/2 coherence analysis is based on 261 coherence maps (139 from track 240 and 122 from track 011) that were generated using 51 ERS-1/2 SAR images. Similar to the RADARSAT behavior, ERS-1/2 coherence also shows strong dependence of temporal baseline. At small temporal baseline ($<$ 35-day), particularly tandem pairs with a 1-day repeat cycle, all wetland vegetation types produce high coherence values. ERS-1/2 coherence of all wetland types degrades quickly within 35–70 days, indicating a strong temporal decorrelation. In herbaceous wetlands, a

coherence level beyond 70 days is very low (< 0.2) and cannot maintain interferometric phase. In woody wetlands, the phase decorrelation threshold is reached within 140 days. Unlike in the JERS and RADARSAT-1 analyses, we were not able to calculate expected coherence values because RMS errors were too large to fit to the simple approximation model mainly due to significant temporal decorrelation.

C. Coherence Comparison Between Spaceborne SAR Systems

We compare between the three SAR systems by plotting for each vegetation class all calculated coherence values as a function of perpendicular and temporal baselines (see Fig. 7). A baseline component was normalized by critical a baseline of each satellite to accommodate the comparison between different spaceborne SAR systems. The theoretical critical baseline (Bc) was computed as in [18] and [41]. Bc is around 1100 m for ERS-1/2 and ENVISAT, and 6.5 and 6 km for JERS-1 and RADARSAT-1 fine beam modes, respectively.

In general, JERS-1 has the best coherence among the four systems for all wetland vegetation types; ERS-1/2 has much lower coherence, and the coherence value for RADARSAT-1 lie in between those of JERS-1 and ERS-1/2. Although we have a small ENVISAT data set (four scenes only), our analysis indicates that ENVISAT signals have slightly better coherence than ERS-1/2. ENVISAT coherence in sawgrass is comparable with RADARSAT-1, but in the other vegetation classes, ENVISAT has lower coherence than RADARSAT-1. The ENVISAT ASAR differs from the ERS-1/2 SAR in the radar polarization (HH for ENVISAT and VV for ERS-1/2), and has a slight difference of incidence angle (28.7° for ENVISAT and 23° for ERS-1/2), whereas wavelength (C-band) and spatial resolution are almost the same in both systems. The higher coherence of the HH polarization ENVISAT data suggests that HH polarization is more effective for wetland InSAR application. Early studies showed that the enhanced backscattering in wetlands is mainly the product of double-bounce scattering between an underlying smooth water surface and trunks and branches [1]. Double-bounce backscattering at HH is stronger and more coherent than at VV because of the stronger reflection induced by the Fresnel reflection coefficient over water for HH polarization ([45], [46]). In fact, reflection coefficients on trunk and ground surface (or water in wetlands) play an important role for the backscattering intensity. HH backscatter is usually four to six times stronger than VV for the trunk–ground structure [46]. The difference in coherence with polarization had been also reported in studies of SIR-C [9], [47] and TerraSAR-X data [17]. Both RADARSAT-1 and ENVISAT have C-band wavelength and HH polarization, but they have different resolution; the difference of incidence angle (ENVISAT with steep incidence angle might be more favorable) is almost negligible. High spatial resolution such as RADARSAT-1 fine beam mode appears to produce high coherence. Fig. 7 clearly supports that JERS-1 with L-band and HH polarization is the best system for the detection of water-level change using interferometric phase in all wetland vegetation types (herbaceous and woody wetlands), and high-resolution RADARSAT-1 with C-band and HH polarization is the second best.

D. Coherence Levels in Relation to the SAR Backscatter Coefficient

We investigate the relations between a backscatter coefficient and a coherence level by calculating the mean values for the five wetland classes. As in the previous coherence analyses, we use data from the "stable areas" in order to minimize seasonal effects. Mean backscatter images [see Fig. 8(a)–(c)] were generated by averaging all available geocoded multitemporal backscatter images, whereas the mean coherence image were generated from several good interferograms with small spatial baseline and short acquisition time interval in order to highlight the coherence variation depending on vegetation types. We selected 36 ERS-1/2 interferometric pairs with less than 200 m ($\sim B_c \ / \ 6$) perpendicular baseline and less than 120-day time interval to generate mean coherence image [see Fig. 8(e)]. Similarly, the mean coherence images of JERS-1 and RADARSAT [see Fig. 8(d) and (f)] were generated from 4 and 28 interferograms with a time period of less than 120 days and perpendicular baseline of less than 1 km ($\sim B_c \ / \ 6$).

The three mean backscatter images show similar patterns of high scattering values in the eastern and western sections of South Florida and variable values in the central part [see Fig. 8(a)–(c)]. These backscattering characteristics similar to those reported in previous backscattering studies on wetlands [2], [3], [37], [38]. The high backscattering values (brighter) in the western part occur over the cypress and mixed shrubs wetlands in the BCPN area (see Figs. 1 and 3), whereas the high values in the eastern part occur mostly over the Miami Fort Lauderdale urban area and also over unclassified hammock hardwood (mixed shrub) vegetation in the southeastern part of the Everglades [white area in Fig. 3(b)]. The lower (darker) and variable mean backscattering values occur in the central part of South Florida over herbaceous wetlands in the WCA and ENP areas. The scattering level in these herbaceous wetlands is lowest (darkest) for JERS-1, intermediate for ERS-1/2, and highest (brightest) for RADARSAT. Some of the sawgrass marsh area of a triangular shape in the RADARSAT image [see Fig. 8(c)] is as bright as the urban area to its east. In all three mean backscatter images, the mangrove wetlands occupying most of the western shores show an intermediate scattering level, lower than the cypress and mixed shrubs in the western part and higher than the herbaceous wetlands in the central part of South Florida.

The mean coherence images show an overall similar spatial pattern to the mean backscatter images but with sharper contrast (see Fig. 8). The mean coherence images show a high coherence level (bright) in the western woody wetlands of the BCNP and in the urban areas. They also show a low coherence level (darker) in the central herbaceous wetlands and variable coherence level in the mangrove area along the western shores.

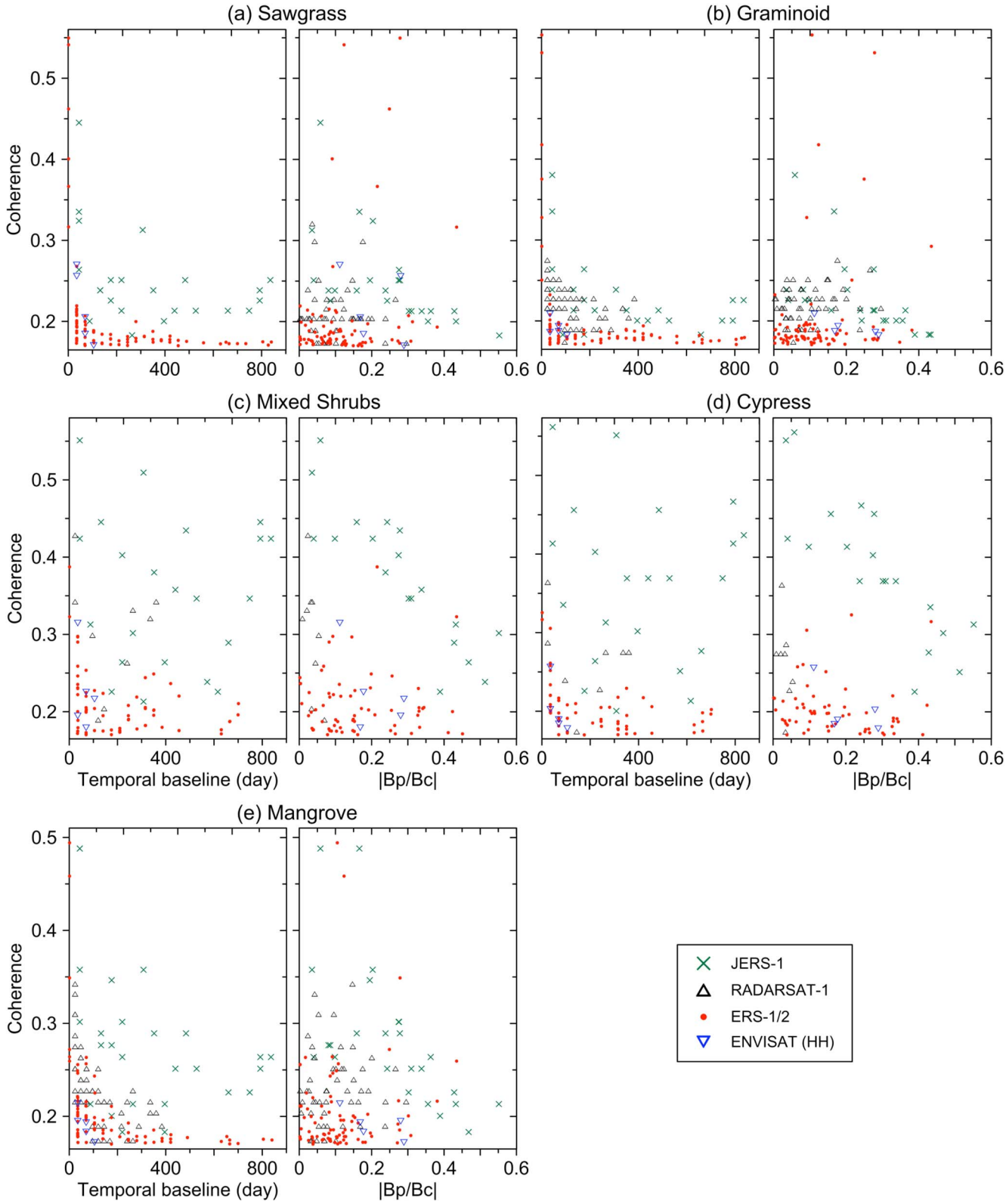

Fig. 7. Comparison between the coherence obtained with the JERS-1, RADARSAT, ERS, and ENVISAT SAR data for each of the five wetland classes as a function of temporal and perpendicular baselines. The perpendicular baseline is normalized by the critical baseline of each SAR system.

We conducted a quantitative comparison between the mean backscatter and coherence for all five wetland types (see Fig. 9). Backscattering intensity of JERS-1 and RADARSAT-1 resulted in almost the same mean (within only 1 dB difference) and deviation, except for sawgrass wetland. Over all classes ERS backscatter was lower than RADARSAT-1 by

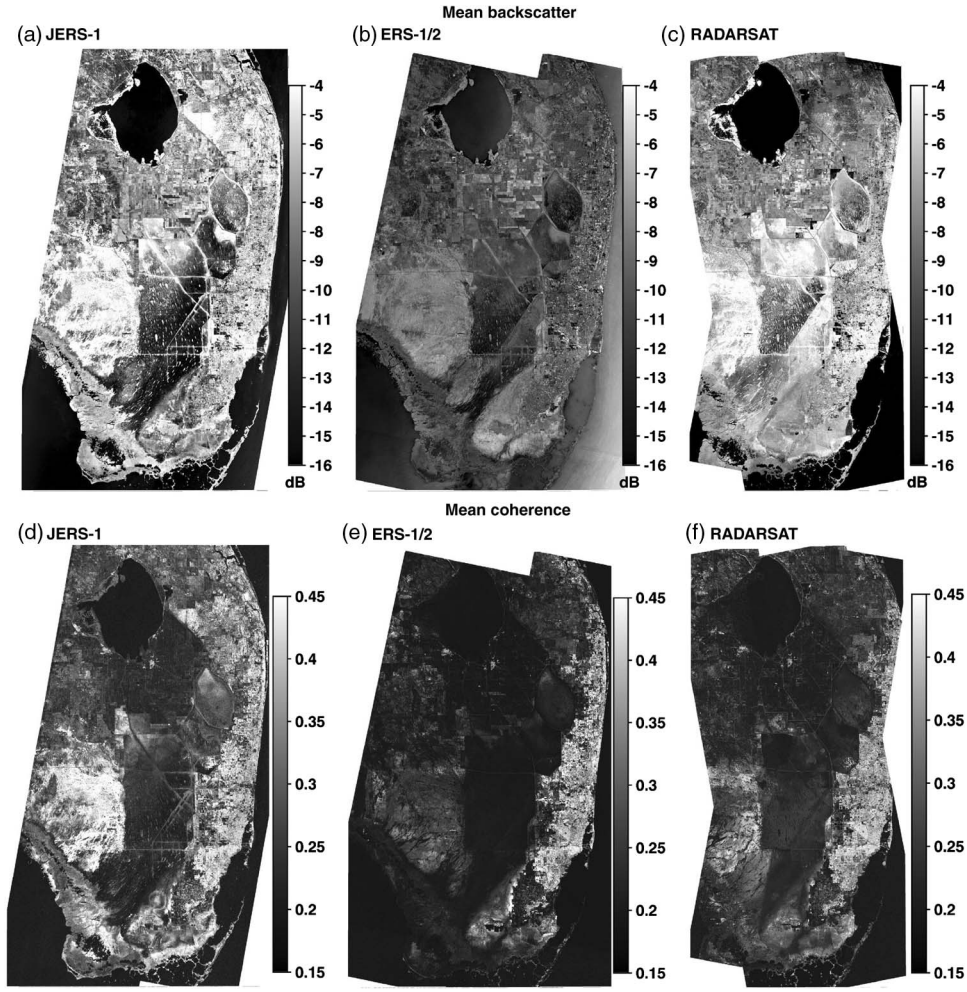

Fig. 8. (Top) (a) Mean SAR backscatter images of JERS-1, (b) ERS-1/2, and (c) RADARSAT fine beam mode. (Bottom) Mean coherence images of (d) 25 JERS-1 SAR interferometric pairs with less than 3-km perpendicular baseline, (e) 36 ERS-1/2 SAR pairs with less than 200-m baseline and 120-day time interval, and (f) 36 RADARSAT fine beam mode pairs with less 1 km baseline and 120 days.

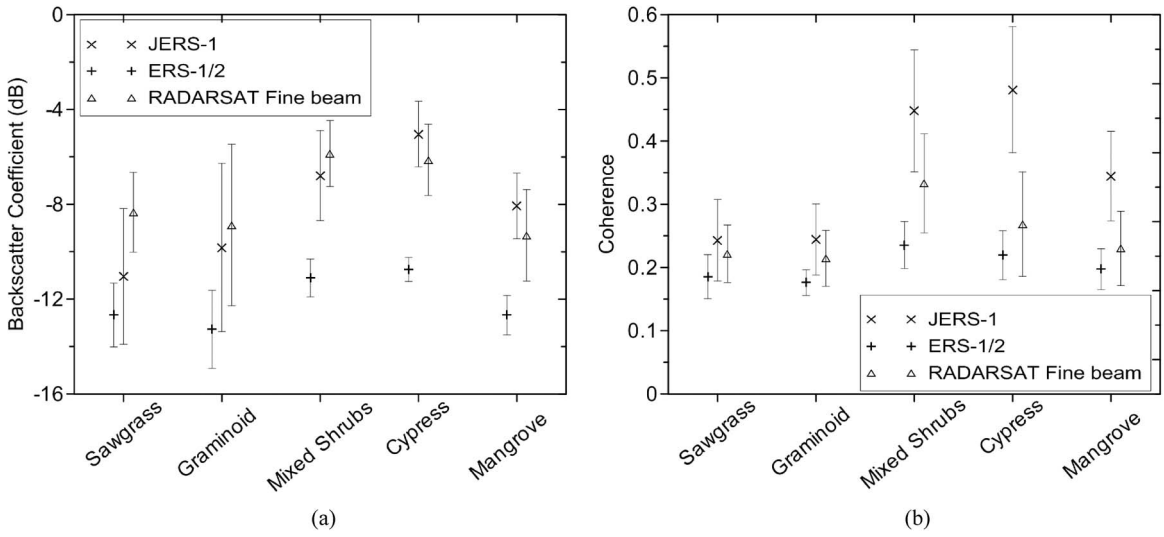

Fig. 9. Mean backscatter coefficients and coherence of the five wetland classes. The vertical bars mark the range of one standard deviation of the mean values. All classes show relative coherence levels with respect to each satellite system. The range of JERS, RADARSAT, ERS SAR coherence mean and backscatter coefficient mean with one standard deviation values from each wetland classes.

3-5 dB, but the variation trend in terms of vegetation class was very similar. Mixed shrubs and cypress produced higher backscatter coefficient in all satellite systems, whereas sawgrass, graminoid, and mangrove (except JERS-1) had lower backscatter. The L-band JERS-1 mean backscatter is lowest over sawgrass marsh and relatively high over mangrove swamp.

Based on Fig. 9, we come to the conclusion that the coherences of cypress and mixed shrubs are higher than that of herbaceous wetlands, and JERS-1 coherence over mangrove swamps has intermediate values, between cypress and herbaceous marshes.

A backscatter coefficient depends on a combination of several wetland properties, including biomass, vegetation height, soil moisture, flooded water level, and vegetation density [5]–[7], [37], [39], [48]. Therefore, it is also interesting to examine the relationship between backscatter and coherence. The results of our analysis are presented in Fig. 10, by plotting the estimated mean coherence with standard deviation against the mean backscattering values for the five vegetation classes. The most intriguing result is that ERS backscatters show no relation to coherence, except in sawgrass marsh, whereas backscatters from JERS-1 and RADARSAT-1 show close relations to coherence in four wetland vegetation types (sawgrass, cypress, mixed shrubs, and mangrove).

The JERS-1 analysis indicates an almost linear relations between coherence and backscattering at low scattering (-18 to -10 dB) levels [see Fig. 10(a)]. The linear relations between the two observables continue for the woody wetlands (cypress and mixed shrubs) and to some degree for mangroves and sawgrass at higher scattering levels. However, coherence over graminoid wetlands becomes saturated at about 0.3 and hence shows no linear correlation with backscattering at higher backscattering levels. For JERS-1, high coherence is a good indicator for a high backscatter coefficient, but a high backscatter coefficient does not always produce high coherence in herbaceous wetlands [see Fig. 10(a)].

For RADARSAT-1, the correlation between coherence and backscatter coefficient is less pronounced than for the JERS-1. At lower backscatter values (< -8 dB), there is no correlation between the two observables [see Fig. 10(b)]. Nevertheless, a general increase in the coherence after about -8 dB is identified, except for graminoid. Similar to the results of JERS-1, high coherence levels are generally indicators for high backscatter levels, particularly in woody wetlands. However, backscatter levels are not good indicator for coherence levels. The ERS-1/2 analysis yields no significant correlation between backscattering and coherence [see Fig. 10(c)]. The coherence level at all vegetation types is low (0.2–0.3) and not indicative of the much wider backscattering range extending from -18 to -10 dB.

The positive backscattering–coherence correlation found for the JERS-1 and RADARSAT data suggests that the relations between these two observables have stronger dependence on polarization than on the radar wavelength. Double-bounce scattering in HH polarization is much stronger than in VV polarization [13], [46]. Backscattering in ERS-1/2 with short wavelength and VV polarization might be dominated by volume scattering from leaves and canopies of vegetation, as shown in [49]. Table III summarizes the correlation coefficients between the mean backscatter coefficient and the mean coherence image for each satellite according to the five vegetation types. JERS-1 backscatter correlates relatively well with coherence of 0.33–0.66 for all wetland types. For RADARSAT-1, the correlations of woody wetlands (0.21–0.66) are as high as

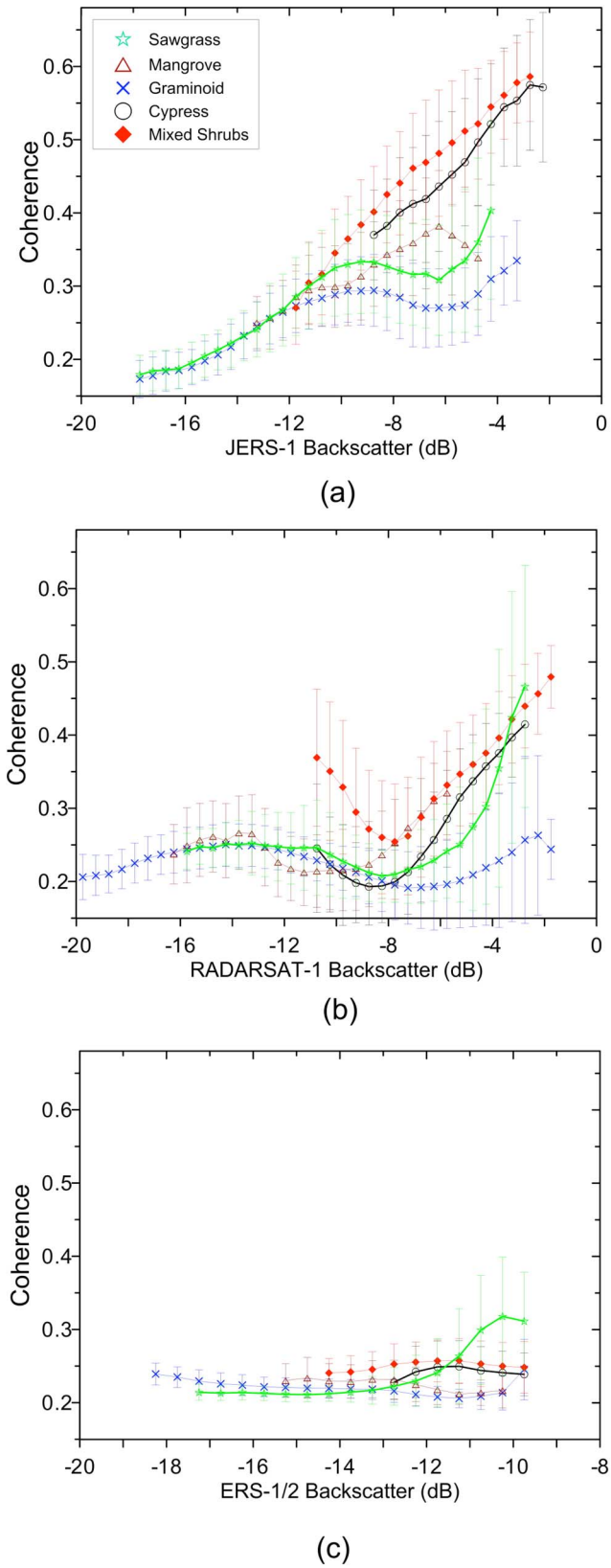

Fig. 10. Relations between mean interferometric coherence and mean backscatter for several wetland vegetation classes according to satellite systems: (a) JERS-1, (b) RADARSAT, and (c) ERS-1/2. Vertical line marks one standard deviation of coherence estimation.

TABLE III
SUMMARY OF CORRELATION COEFFICIENTS BETWEEN MEAN BACKSCATTER AND MEAN COHERENCE FOR FIVE MARSH AREAS IN THE SOUTH FLORIDA

Satellite \ Marsh type	Sawgrass	Graminoid	Mixed Shrubs	Cypress	Mangrove	All marshes
JERS-1	0.66	0.45	0.58	0.49	0.33	0.64
RADARSAT (all)	0.02	-0.32	0.45	0.66	0.21	0.31
RADARSAT (>-8dB)*	0.34	0.11	0.48	0.66	0.31	0.54
ERS-1/2	0.41	-0.35	0.00	-0.07	-0.21	0.22

* The value in parentheses represents the correlation coefficient derived from pixels with backscatter larger than -8 dB

that by JERS-1, but significantly lower at herbaceous wetlands. The results suggest that the correlation between coherence and the backscatter coefficient over wetlands is best obtained with L-band HH-polarization.

V. CONCLUSION

We used a total of 90 repeat-pass JERS-1, ERS-1/2, RADARSAT-1, and ENVISAT SAR data acquisitions to calculate coherence variations for five typical wetland vegetation types (sawgrass, graminoid, cypress, mixed shrubs, and mangrove) in South Florida. To minimize the effect of water-level changes on coherence at multitemporal data, we conducted our analysis for each vegetation class on selected areas with low backscatter deviation as indicators for stable wetland extent. Statistics were extracted and then analyzed in connection with temporal and perpendicular baselines, as well as polarization, incidence angle, and pixel resolution. The main conclusions of our coherence analysis are as follows:

1) Freshwater woody wetlands (cypress and mixed shrubs swamps) have higher coherence levels than herbaceous wetlands (sawgrass and graminoid marshes). Saltwater woody mangrove wetlands have intermediate coherence values, higher than those of the herbaceous wetlands, but lower than those of the freshwater woody ones.
2) The coherence level of L-band data depends mainly on perpendicular baseline. In herbaceous wetlands, the coherence also depends on temporal baseline. In herbaceous wetlands, interferometric phase (coherence > 0.2) can be maintained over six month and even longer, depending on volume decorrelation by the perpendicular baseline. In woody wetlands, the phase can be maintained even after three years.
3) The coherence level of C-band data is strongly dependent on temporal baseline. Due to the fast decorrelation of the ERS-1/2 C-VV data, interferometric phase (coherence > 0.2) can be maintained in herbaceous wetlands only over short temporal baselines (< 70 days). The RADARSAT C-HH data can maintain the phase in herbaceous wetlands over longer time periods, extending over 72 days and even 96 days. In woody wetlands, ERS-1/2 can maintain a coherent phase within 70 days, whereas RADARSAT maintains a phase after a year.
4) A comparative analysis between coherence and the backscattering coefficient indicates that backscattering from JERS-1 and RADARSAT-1 is correlated with coherence in four wetland vegetation types (sawgrass, cypress, mixed shrubs and mangrove). However, ERS-1/2 backscattering has no relation to coherence, except over sawgrass marsh, most likely due to dominant volume scattering from leaves and canopies.
5) Based on our coherence analysis, we conclude that high resolution, HH polarization, and small incidence angle observations are most suitable for the wetland InSAR applications.

ACKNOWLEDGMENT

The authors would like to thank NASA and the Office of Naval Research for support, the European Space Agency for access to the ERS data, Radarsat International, Inc. for the RADARSAT-1 data, SFWMD for the land cover vector map, and the three anonymous reviewers for their helpful reviews.

REFERENCES

[1] J. A. Richards, P. W. Woodgate, and A. K. Skidmore, "An explanation of enhanced radar backscattering from flooded forests," *Int. J. Remote Sens.*, vol. 8, no. 7, pp. 1093–1100, Jul. 1987.
[2] K. O. Pope, J. M. Reybenayas, and J. F. Paris, "Radar remote-sensing of forest and wetland ecosystems in the Central-American tropics," *Remote Sens. Environ.*, vol. 48, no. 2, pp. 205–219, May 1994.
[3] L. L. Hess, J. M. Melack, S. Filoso, and Y. Wang, "Delineation of inundated area and vegetation along the Amazon flood plain with the SIR-C synthetic aperture radar," *IEEE Trans. Geosci. Remote Sens.*, vol. 33, no. 4, pp. 896–904, Jul. 1995.
[4] E. S. Kasischke and L. L. Bourgeau-Chavez, "Monitoring South Florida wetlands using ERS-1 SAR imagery," *Photogramm. Eng. Remote Sens.*, vol. 63, no. 3, pp. 281–291, Mar. 1997.
[5] L. L. Bourgeau-Chavez, K. B. Smith, S. M. Brunzell, E. S. Kasischke, E. A. Romanowicz, and C. J. Richardson, "Remote monitoring of regional inundation patterns and hydroperiod in the greater everglades using synthetic aperture radar," *Wetlands*, vol. 25, no. 1, pp. 176–191, Mar. 2005.
[6] L. L. Hess, J. M. Melack, and D. S. Simonett, "Radar detection of flooding beneath the Forest Canopy—A review," *Int. J. Remote Sens.*, vol. 11, no. 7, pp. 1313–1325, Jul. 1990.
[7] Y. Wang, L. L. Hess, S. Filoso, and J. M. Melack, "Understanding the radar backscattering from flooded and nonflooded Amazonian forests: Results from canopy backscatter modeling," *Remote Sens. Environ.*, vol. 54, no. 3, pp. 324–332, Dec. 1995.
[8] W. P. Waite and H. C. MacDonald, "Vegetation penetration with K-band imaging radars," *IEEE Trans. Geosci. Electron.*, vol. GE-9, no. 3, pp. 147–155, Jul. 1971.

[9] D. E. Alsdorf, J. M. Melack, T. Dunne, L. A. K. Mertes, L. L. Hess, and L. C. Smith, "Interferometric radar measurements of water level changes on the Amazon flood plain," *Nature*, vol. 404, no. 6774, pp. 174–177, Mar. 2000.

[10] S. W. Kim, S. H. Hong, and J. S. Won, "An application of L-band synthetic aperture radar to tide height measurement," *IEEE Trans. Geosci. Remote Sens.*, vol. 43, no. 7, pp. 1472–1478, Jul. 2005.

[11] S. Wdowinski, F. Amelung, F. Miralles-Wilhelm, T. H. Dixon, and R. Carande, "Space-based measurements of sheet-flow characteristics in the Everglades wetland, Florida," *Geophys. Res. Lett.*, vol. 31, no. 15, pp. L15 503-1–L15 503-5, Aug. 2004.

[12] S. Wdowinski, S. W. Kim, F. Amelung, T. H. Dixon, F. Miralles-Wilhelm, and R. Sonenshein, "Space-based detection of wetlands' surface water level changes from L-band SAR interferometry," *Remote Sens. Environ.*, vol. 112, no. 3, pp. 681–696, Mar. 2008.

[13] J.-W. Kim, Z. Lu, H. Lee, C. K. Shum, C. M. Swarzenski, T. W. Doyle, and S.-H. Baek, "Integrated analysis of PALSAR/Radarsat-1 InSAR and ENVISAT altimeter data for mapping of absolute water level changes in Louisiana wetlands," *Remote Sens. Environ.*, vol. 113, no. 11, pp. 2356–2365, Nov. 2009.

[14] Z. Lu and O. I. Kwoun, "Radarsat-1 and ERS InSAR analysis over southeastern coastal Louisiana: Implications for mapping water-level changes beneath swamp forests," *IEEE Trans. Geosci. Remote Sens.*, vol. 46, no. 8, pp. 2167–2184, Aug. 2008.

[15] S. H. Hong, S. Wdowinski, S. W. Kim, and J. S. Won, "Space-based multitemporal monitoring of wetland water levels: Case study of WCA1 in the Everglade," *Remote Sens. Environ.*, vol. 114, no. 11, pp. 2436–2447, Nov. 2010.

[16] B. R. N. Gondwe, S. H. Hong, S. Wdowinski, and P. Bauer-Gottwein, "Hydrologic dynamics of the ground-water-dependent Sian Ka'an wetlands, Mexico, derived from InSAR and SAR data," *Wetlands*, vol. 30, no. 1, pp. 1–33, Feb. 2010.

[17] S. H. Hong, S. Wdowinski, and S. W. Kim, "Evaluation of TerraSAR-X observations for Wetland InSAR application," *IEEE Trans. Geosci. Remote Sens.*, vol. 48, no. 2, pp. 864–873, Feb. 2010.

[18] H. A. Zebker and J. Villasenor, "Decorrelation in interferometric radar echoes," *IEEE Trans. Geosci. Remote Sens.*, vol. 30, no. 5, pp. 950–959, Sep. 1992.

[19] U. Wegmuller and C. L. Werner, "SAR interferometric signatures of Forest," *IEEE Trans. Geosci. Remote Sens.*, vol. 33, no. 5, pp. 1153–1161, Sep. 1995.

[20] J. O. Hagberg, L. M. H. Ulander, and J. Askne, "Repeat-pass SAR interferometry over forested terrain," *IEEE Trans. Geosci. Remote Sens.*, vol. 33, no. 2, pp. 331–340, Mar. 1995.

[21] J. I. H. Askne, P. B. G. Dammert, L. M. H. Ulander, and G. Smith, "C-band repeat-pass interferometric SAR observations of the forest," *IEEE Trans. Geosci. Remote Sens.*, vol. 35, no. 1, pp. 25–35, Jan. 1997.

[22] C. Hall-Atkinson and L. C. Smith, "Delineation of delta ecozones using interferometric SAR phase coherence Mackenzie River Delta, NWT, Canada," *Remote Sens. Environ.*, vol. 78, no. 3, pp. 229–238, Dec. 2001.

[23] D. J. Weydahl, "Analysis of ERS SAR coherence images acquired over vegetated areas and urban features," *Int. J. Remote Sens.*, vol. 22, no. 14, pp. 2811–2830, Jan. 2001.

[24] D. J. Weydahl, "Analysis of ERS tandem SAR coherence from glaciers, valleys, and Fjord Ice on Svalbard," *IEEE Trans. Geosci. Remote Sens.*, vol. 39, no. 9, pp. 2029–2039, Sep. 2001.

[25] R. F. Doren, K. Rutchey, and R. Welch, "The Everglades: A perspective on the requirements and applications for vegetation map and database products," *Photogramm. Eng. Remote Sens.*, vol. 65, no. 2, pp. 155–161, Feb. 1999.

[26] "South Florida Multi-Species Recovery Plan," Atlanta, GA, 1999.

[27] I. Olmsted and T. V. Armentano, "Vegetation of Shark Slough, Everglades National Park," South Florida Natural Resources Center, Homestead, FL, Tech. Rep. 97-001, 1997.

[28] *lscndclu99*, Avineon Inc., Alexandria, VA, 2005.

[29] C. Homer, C. Q. Huang, L. M. Yang, B. Wylie, and M. Coan, "Development of a 2001 national land-cover database for the United States," *Photogramm. Eng. Remote Sens.*, vol. 70, no. 7, pp. 829–840, Jul. 2004.

[30] *APEX 2002 User's Manual VX-APEX-001*, Vexcel Corporation, Boulder, CO, 2004.

[31] N. Shepherd, "Extraction of Beta-Nought and Sigma-Nought from RADARSAT CDPF Products," ALTRIX Syst., Ontario, Canada, CSA Doc. AS97-5001, 2000.

[32] S. M. Buckley, P. A. Rossen, and P. Persaud, "ROI_PAC Documentation—Repeat Orbit Interferometry Package," JET Propulsion Lab., Pasadena, CA, 2000.

[33] R. Touzi, A. Lopes, J. Bruniquel, and P. W. Vachon, "Coherence estimation for SAR imagery," *IEEE Trans. Geosci. Remote Sens.*, vol. 37, no. 1, pp. 135–149, Jan. 1999.

[34] D. Geudtner and M. Schwabisch, "'flat earth' phase removal, phase-to-height conversion, and geocoding of InSAR-derived DEMs," in *Proc. EUSAR*, Konogswinter, Germany, 1996, pp. 249–252.

[35] P. A. Rosen, S. Hensley, I. R. Joughin, F. K. Li, S. N. Madsen, E. Rodriguez, and R. M. Goldstein, "Synthetic aperture radar interferometry," *Proc. IEEE*, vol. 88, no. 3, pp. 333–382, Mar. 2000.

[36] U. Wegmuller, "Automated terrain corrected SAR geocoding," in *Proc. IEEE IGARSS*, Hamburg, Germany, 1999, pp. 1712–1714.

[37] K. O. Pope, E. Rejmankova, J. F. Paris, and R. Woodruff, "Detecting seasonal flooding cycles in marshes of the Yucatan Peninsula with SIR-C polarimetric radar imagery," *Remote Sens. Environ.*, vol. 59, no. 2, pp. 157–166, Feb. 1997.

[38] M. P. F. Costa, O. Niemann, E. Novo, and F. Ahern, "Biophysical properties and mapping of aquatic vegetation during the hydrological cycle of the Amazon floodplain using JERS-1 and Radarsat," *Int. J. Remote Sens.*, vol. 23, no. 7, pp. 1401–1426, Jan. 2002.

[39] E. S. Kasischke, K. B. Smith, L. L. Bourgeau-Chavez, E. A. Romanowicz, S. Brunzell, and C. J. Richardson, "Effects of seasonal hydrologic patterns in south Florida wetlands on radar backscatter measured from ERS-2 SAR imagery," *Remote Sens. Environ.*, vol. 88, no. 4, pp. 423–441, Dec. 2003.

[40] A. Ferretti, C. Colesanti, D. Perissin, C. Prati, and F. Rocca, "Evaluating the effect of the observation time on the distribution of SAR permanent scatterers," in *Proc. FRINGE*, Frascati, Italy, 2003, pp. 1–5.

[41] F. Gatelli, A. M. Guarnieri, F. Parizzi, P. Pasquali, C. Prati, and F. Rocca, "The wave-number shift in SAR interferometry," *IEEE Trans. Geosci. Remote Sens.*, vol. 32, no. 4, pp. 855–865, Jul. 1994.

[42] A. Refice, F. Bovenga, and R. A. Nutricato, "MST-based stepwise connection strategies for multipass radar data, with application to coregistration and equalization," *IEEE Trans. Geosci. Remote Sens.*, vol. 44, no. 8, pp. 2029–2040, Aug. 2006.

[43] M. Simard, S. Hensley, M. Lavalle, R. Dubayah, N. Pinto, and M. Hofton, "An empirical assessment of temporal decorrelation using the uninhabited aerial vehicle synthetic aperture radar over forested landscapes," *Remote Sens.*, vol. 4, no. 4, pp. 975–986, Apr. 2012.

[44] R. M. Hoffer, D. F. Lozano-Garcia, and D. D. Gillespie, "Characterizing forest stands with multi-incidence angle and multi-polarized SAR data," *Adv. Space Res.*, vol. 7, no. 11, pp. 309–312, Nov. 1987.

[45] F. Ribbes and T. Le Toan, "Rice field mapping and monitoring with RADARSAT data," *Int. J. Remote Sens.*, vol. 20, no. 4, pp. 745–765, Mar. 1999.

[46] Y. H. Dong, B. C. Forster, and C. Ticehurst, "A new decomposition of radar polarization signatures," *IEEE Trans. Geosci. Remote Sens.*, vol. 36, no. 3, pp. 933–939, May 1998.

[47] D. E. Alsdorf, L. C. Smith, and J. M. Melack, "Amazon floodplain water level changes measured with interferometric SIR-C radar," *IEEE Trans. Geosci. Remote Sens.*, vol. 39, no. 2, pp. 423–431, Feb. 2001.

[48] J. A. Richards, G. Q. Sun, and S. S. Simonett, "L-band radar backscatter modeling of forest stands," *IEEE Trans. Geosci. Remote Sens.*, vol. 25, no. 4, pp. 487–498, Jul. 1987.

[49] S. R. Cloude, "Dual-baseline coherence tomography," *IEEE Geosci. Remote Sens. Lett.*, vol. 4, no. 1, pp. 127–131, Jan. 2007.

Sang-Wan Kim (S'00–M'05) received the Ph.D. degree in Earth system sciences from Yonsei University, Seoul, Korea, in 2004. His Ph.D. thesis was on the analysis of subsidence in the urban area using permanent scatterer and volcano monitoring using differential InSAR.

He is currently an Assistant Professor with the Department of Geoinformation Engineering, Sejong University, Korea. His research interests include SAR data processing, application of SAR interferometry, and high-resolution SAR and InSAR application in urban area and geohazard monitoring.

Shimon Wdowinski received the B.Sc. degree in Earth sciences and M.Sc. degree in geology from the Hebrew University, Jerusalem, Israel, in 1983 and 1985, respectively, and M.S. degree in engineering sciences and Ph.D. degree in geophysics from Harvard University, Boston, MA, in 1988 and 1990, respectively.

He is currently a Research Associate Professor with the Division of Marine Geology and Geophysics, the Rosenstiel School of Marine and Atmospheric Science, University of Miami, Coral Gables, FL, USA. He is a Principal Investigator of projects funded by NASA, ESA, Canadian Space Agency, German Space Agency, and Italian Space Agency on studies using SAR and InSAR observations for wetland research. His research interests include the development and usage of space geodetic techniques that can detect very precisely small movements on the Earth's surface. He successfully applied these technologies to study natural hazards and environmental phenomena, such as earthquakes, sea-level rise, landslides, urban subsidence, and wetland surface flow.

Falk Amelung received the M.S. degree in geophysics from the University of Muenster, Muenster Germany, in 1992 and the Ph.D. degree from the University of Strasbourg, Strasbourg, France, in 1996.

He worked as a Research Scientist with Stanford University, Stanford, CA, USA, and with the University of Hawaii, Honolulu, HI. Then, in 2002, he was with the University of Miami, Coral Gables, FL, USA. He is currently a Professor of geophysics with the Division of Marine Geology and Geophysics, Rosenstiel School of Marine and Atmospheric Sciences, University of Miami, Coral Gables, FL. His research interests include InSAR studies of active volcanism, active tectonics, land subsidence, and the use of InSAR for measuring subtle tectonic deformation and for volcano monitoring.

Dr. Amelung is currently the Chair for the Scientific Advisory Committee of Group on Earth Observation's Geohazard Supersites and Natural Laboratory initiative.

Timothy H. Dixon received the B.Sc. degree from the University of Western Ontario, London, ON, Canada, in 1974 and the Ph.D. degree from the University of California at San Diego, San Diego, CA, USA.

From 1979 to 1992, he worked with the Jet Propulsion Laboratory, NASA, Pasadena, CA, USA. From 1992 to 2010, he was a Professor with the University of Miami, Coral Gables, FL, USA, where he cofounded the Center for Southeastern Tropical Advanced Remote Sensing. Since January 2011 he has been with the University of South Florida, Tampa, FL, where he is currently a Professor with the Department of Geology. His research interests include earthquakes and volcano deformation, coastal subsidence, ground water extraction, and glacier motion.

Dr. Dixon was a Distinguished Lecturer for the American Association of Petroleum Geologists (2006–2007). He is currently a Fellow of the American Geophysical Union and the Geological Society of America (GSA). He was a recipient of the GSA "Best Paper" Award in 2006, and the GSA's Woollard Award in 2010.

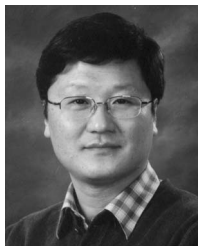

Joong-Sun Won (S'92–M'93–SM'03) received the B.S. and M.S. degrees in geology and geophysics from Yonsei University, Seoul, Korea, in 1983 and 1985, respectively, and the Ph.D. degree in geophysics from the University of Manitoba, Winnipeg, MB, Canada, in 1993.

From 1993 to 1996, he was a Senior Scientist with the Marine Geology Division, Korea Ocean Research and Development Institute, Ansan, Korea. He is currently a Professor with the Department of Earth System Sciences, Yonsei University. His research interests include remote sensing, tidal flats, geohazard, signal processing, radar interferometry, and velocity retrieval from SAR data.